

Finding massive double-exponential disk galaxies with extended low surface brightness stellar disk - an IllustrisTNG exploration

SUCHIRA SARKAR¹ AND KANAK SAHA¹

¹*Inter-University Centre for Astronomy & Astrophysics, Pune-411007, Maharashtra, India*

ABSTRACT

We study massive disk galaxies (stellar mass $\geq 10^{11}M_{\odot}$) at $z=0$ from IllustrisTNG simulation to detect galaxies that contain two exponential stellar disks - a central high surface brightness (HSB) disk surrounded by an extended low surface brightness (LSB) envelope. This is motivated by observation of several giant LSB galaxies, reported in literature, showing such complex layered structure (e.g, Malin 1, UGC 1378, UGC 1382 etc). We use the high resolution IllustrisTNG50 data, and perform Sersic plus exponential profile modeling on the idealised, synthetic SDSS-g, r band images of the massive disk galaxies using GALFIT. We identify 7 disk galaxies (12% of the parent sample of disk galaxies) that are best represented by a central Sersic plus a central HSB disk surrounded by an extended LSB disk. The radial scale lengths of the LSB disk lie in the range of ~ 9.7 - 31.7 kpc in agreement to that found in literature. We study the star formation properties of these simulated double-disk galaxies to understand the distribution of these from blue star-forming to red-quenched region. Some of these double-disk galaxies display a characteristic minima in their (g-r) color radial profiles. The double-disk galaxies are found to lie within $\sim 1.5\sigma$ region of the Baryonic Tully-Fisher relation from observation. Our theoretical exploration will be potentially useful in exploring the faint outskirts of massive disk galaxies in upcoming deep surveys such as LSST.

Keywords: Galaxies (573) — Galaxy disks(589)— Giant galaxies(652) — Low surface brightness galaxies(940) —Galaxy formation(595)

1. INTRODUCTION

The formation of the most massive disk galaxies (total stellar mass $\sim 10^{11}M_{\odot}$) in the nearby universe ($z < 0.1$) represents an important open question in the current research in extra-galactic astrophysics. One extreme class of the massive disk galaxies are the "giant low surface brightness" galaxies. A stellar disk is termed as a low surface brightness (LSB) disk if its central surface brightness is > 22.5 mag.arcsec⁻² in the optical B-band (McGaugh 1996; Rosenbaum et al. 2009). The giant LSB galaxies typically harbour stellar disk of exponential scale length more than about 10 kpc (Sprayberry et al. 1995; Das 2013; Saburova et al. 2023; Zhu et al. 2023). Malin 1, a massive ($\log(M_{\star}/M_{\odot})=11.9$), prototypical giant LSB galaxy was observed to contain a large stellar disk extending upto ~ 100 kpc in radius

(Moore & Parker 2006), with an extrapolated central surface brightness of ~ 25.5 mag arcsec⁻² in V- band (Bothun et al. 1987; Impey & Bothun 1989). Till date, Malin 1 remains the most elusive example of a giant LSB galaxy which invokes challenging questions regarding massive disk galaxy formation scenario. Interestingly, Barth (2007) discussed that the morphology of Malin 1 should be best described using a central bulge, bar, a high surface brightness exponential disk (HSB) surrounded by an outer extended low surface brightness exponential disk which is photometrically decoupled from the HSB disk. Recently, Saha et al. (2021) studied detailed structural decomposition of Malin 1 using HST and CFHT (Canada-France Hawaii Telescope) g-band observation. The central HSB disk and the outermost extended LSB disk were found to have radial exponential scale lengths of 4.8 (in HST/F814W band) & 47 kpc(in CFHT-g band), respectively. The central region resembles to a lenticular galaxy, and the outer extended disk contains the large spiral structure. They reported an intermediate LSB disk too. Several other galaxies

suchira.sarkar@iucaa.in

kanak@iucaa.in

Table 1. The redshift, central surface brightness (μ_0 , typically in g, r or B band) and radial scale lengths (R_D) of the inner and outer exponential stellar disks of a sample of observed double-exponential disk galaxies. In each case, the outer disks are determined as low surface brightness disks in their corresponding observed band. We note that μ_0 for inner disk in Malin 1 is reported in HST/F814W band.

| Galaxy ID | Redshift(z) | Inner disk | | Outer disk | |
|-----------------------|-------------|---------------------------------------|---------------------|---------------------------------------|---------------------|
| | | $\mu_{0,ID}$ (mag arcsec $^{-2}$) | $R_{D,ID}$ (kpc) | $\mu_{0,OD}$ (mag arcsec $^{-2}$) | $R_{D,OD}$ (kpc) |
| (1) | (2) | (3) | (4) | (5) | (6) |
| Malin 1 ^a | 0.0827 | 17.64 | 4.8 | 26.7 | 47.0 |
| UGC 1378 ^b | 0.0098 | 19.88 | 4.51 | 21.54 | 12.6 |
| UGC 1382 ^c | 0.0186 | 20.1 | 6.0 | 25.8 | 38.0 |
| NGC 2841 ^d | 0.0021 | ~19.0 | 3.1 | ~25.0 | 13.0 |
| IZw 81 ^e | 0.0518 | 20.31 | 2.04 | 23.32 | 7.35 |

^aSaha et al. (2021), ^bSaburova et al. (2019), ^cHagen et al. (2016), ^dZhang et al. (2018), ^ePandey et al. (2022)

with a double-exponential disk morphology, although less extreme than Malin 1, were discovered over the last decade. UGC 1382, classified as a gLSB ($R \sim 80$ kpc) by Hagen et al. (2016), was found to have a similar morphology of a double-exponential disk structure. The inner HSB and the outer LSB disks were found to have effective radii (R_e) of 6 kpc & 38 kpc, respectively. A few other similar examples include NGC 2841 (Zhang et al. 2018), UGC 1378 (Saburova et al. 2019) etc. Very interestingly, Pandey et al. (2022) reported a lenticular galaxy IZw 81 in the Bootes void region, that contains a HSB and a LSB disk with exponential scale lengths of 2.04 kpc & 7.35 kpc, respectively, and has a smaller radial extent than a typical gLSB. The detailed structural parameters of all the above mentioned galaxies are given in Table 1.

Usually, the most massive galaxies are believed to undergo a morphological transformation from disk to spheroid across cosmic time, and thus the morphology of the most massive galaxies in the nearby universe should be dominated by spheroids. Nevertheless, a significant number of massive disk galaxies are observed in the nearby universe, including the class of gLSBs (Jackson et al. 2020, 2022). The physical process by which such galaxies build their large stellar disk, such as in Malin 1, as well as the survival of such large stellar disk till $z=0$ is hard to comprehend. Further, the presence of double-exponential disk structure as observed pose an even more intriguing question. The photometrically decoupled outer LSB disk could have an ex-situ origin, i.e, it could have been built by the accretion of stars from dwarf satellites, or, could have been built by stars migrated from the inner galaxy via secular evolution process, or, there could be in-situ star formation in the LSB disk itself (as discussed by Hagen et al. (2016); Zhang et al. (2018)). But the detection of a small number of such galaxies in observations prevent us from un-

derstanding their formation mechanism robustly. Such systems could be genuinely rare to form, or, this could be due to the limitation of the detection of the faint outskirts in observations.

The formation of low surface brightness galaxies, containing single exponential LSB stellar disk, has been studied in detail in cosmological hydrodynamical simulation suits, e.g, using NIHAO (Di Cintio et al. 2019), EAGLE (Kulier et al. 2020), IllustrisTNG (Pérez-Montaño et al. 2022) etc. Zhu et al. (2018, 2023) studied gLSBs, containing large, single exponential LSB disk using IllustrisTNG simulation. But a systematic study of double-exponential disk structure remained little explored. The advent of deep and wide photometric data from the ongoing observations such as using the Subaru telescope (Hyper Suprime Cam Subaru Strategic Program (Aihara et al. 2018)), Dragonfly telescope (Abraham & van Dokkum 2014) as well as the upcoming survey such as LSST (Large Synoptic Survey Telescope (Ivezić et al. 2019)), are supposed to increase the detection limit of the low surface brightness regime of galaxies unprecedentedly. In this context, a theoretical study of such double-exponential massive disk galaxies will add important insights in the galaxy formation scenario as well as in the low surface brightness science.

In this paper, we aim to detect the massive double-exponential disk galaxies that have the second outer disk as an extended low surface brightness envelope from IllustrisTNG simulation suit, a cosmological gravomagneto-hydrodynamical simulation (Pillepich et al. 2018a,b). We make use of its highest resolution run, i.e, TNG50-1 (Nelson et al. 2019; Pillepich et al. 2019) and perform morphological bulge+disk decomposition to find such galaxies. We note, that Zhu et al. (2023) primarily did a bulge plus an exponential disk modeling (Sersic plus single exponential) to determine gLSB galaxies, and then also explored if a two-disk fitting is

better than a sersic plus disk fitting. They found that both models are exactly equally good for representing their sample of gLSBs, and therefore describe the galaxies using bulge and single disk. Here, in this paper, we aim to determine galaxies that have a complex layered morphology- a bulge/bar, an inner HSB disk and an outer, extended LSB disk, which has not been theoretically explored yet. The paper is organized as follows. We introduce the simulation details and the method to detect the double disk galaxies from the simulation data in Section 2, the structural and other physical properties of the double-disk galaxies in Section 3, and summarize our results in Section 4.

2. METHODS

2.1. *IllustrisTNG50 simulation*

The IllustrisTNG Project (Nelson et al. 2018; Pillepich et al. 2018a; Springel et al. 2018; Marinacci et al. 2018; Naiman et al. 2018) is a suite of cosmological gravo-magneto-hydrodynamical simulations run using the moving-mesh code AREPO (Springel 2010). It is the successor of the original Illustris simulation (Genel et al. 2014; Vogelsberger et al. 2014a,b; Sijacki et al. 2015). The galaxy formation model employed in the TNG simulation is outlined in Weinberger et al. (2017) and Pillepich et al. (2018a), and is calibrated to reproduce the $z=0$ galaxy stellar mass function, galaxy stellar-to-halo mass relation, galaxy stellar mass-size relation etc. The TNG galaxy formation model is an updated and improved version of the model used in the Illustris project. The IllustrisTNG simulations are run using the cosmologically motivated initial conditions, assuming an updated cosmology consistent with the Planck results (Planck Collaboration et al. 2016), where $\Omega_{\Lambda,0}=0.6911$, $\Omega_{m,0}=0.3089$, $\Omega_{b,0}=0.0486$, $h=0.6774$, $\sigma_8=0.8159$, $n_s=0.9667$. The IllustrisTNG project consists of three simulation volumes. The physical simulation boxes have cubic volumes of roughly 50, 100, and 300 Mpc side length, and the simulations are referred to as TNG50, TNG100, and TNG300, respectively. In this work, we use the data from the highest resolution run, i.e, TNG50-1 (Nelson et al. 2019; Pillepich et al. 2019) which realizes a simulation cube with a volume of 51.7^3 Mpc³, and mean baryonic mass and dark matter particle mass resolution of $8.5 \times 10^4 M_{\odot}$ & $4.5 \times 10^5 M_{\odot}$, respectively. The Plummer equivalent gravitational softening of the collisionless components, i.e, stars, dark matter, is 288 parsecs at $z = 0$. For gas the gravitational softening is adaptive and its minimum is kept at 74 comoving parsecs at all times.

Haloets in TNG simulations are identified using an FoF algorithm, while galaxies (Subhaloes) residing in a halo

are identified using the SUBFIND algorithm (Springel et al. 2001). The volume and the resolution of TNG50-1 is ideal to detect the extended low surface brightness disks in galaxies out of a statistical sample of massive galaxies.

2.2. *Sample selection for massive disk galaxies*

We select all the galaxies (subhaloes) with total stellar mass (defined as the sum of mass of all star particles gravitationally bound to the subhaloes) $\geq 10^{11} M_{\odot}$ at $z=0$, i.e, from snapshot 99 of TNG50-1, and thus obtain an initial parent sample of 132 massive galaxies.

We use the synthetic, idealised SDSS (Sloan Digital Sky Survey)-g,r band images of the above galaxies, made using radiative transfer code SKIRT and available in the TNG supplementary data catalogue (Rodriguez-Gomez et al. 2019), for the morphological measurements. We note that these images in the catalogue, corresponding to $z=0$, were created by assuming that the galaxies are actually located at $z=0.0485$, as would be observed by a local observer. The number of pixels in each image is chosen such that the resulting pixel scale matches that of the observations, i.e, $0.396 \text{ arcsec pixel}^{-1}$ at $z=0.0485$. This corresponds to a linear scale of 0.276 ckpc/h in simulation unit or 0.388 kpc in physical unit, as mentioned in the details of this data catalogue. We note, that the unit of each image is in electron counts $\text{s}^{-1} \text{ pixel}^{-1}$. The magnitude photometric zero-points in AB magnitude system are calculated using $2.5 \log_{10}(\text{fluxmag0})$, where fluxmag0 for SDSS-g, r bands are 2.4×10^{10} , and 2.38×10^{10} electron counts s^{-1} , respectively (as given in TNG website). By construction, each synthetic image contains one galaxy at a random orientation. The field of view is equal to 15 times the 3D stellar half-mass radius of the corresponding galaxy (Rodriguez-Gomez et al. 2019). We note, that these are idealized images as would be hypothetically observed by an instrument with a point-like PSF (i.e. a Dirac delta function), and an infinite signal-to-noise ratio. We do not add any noise or sky background to these images or convolve them with a PSF, and use them in their idealised form only. This makes the images most suitable to detect the extended, low surface brightness outskirts of the galaxies (see Zhu et al. 2023). The observational realism has been found not to have a significant effect on the values of the best-fit parameters of a model (see LaChance et al. (2024)).

First, we visually inspect each galaxy image to identify the ones unsuitable for 2D structural decomposition, especially for identifying the extended low surface brightness disk (e.g., galaxies showing the signature of tidal disturbances/interactions in the outskirts, jets, or appear to be too compact to have a large, second exponential

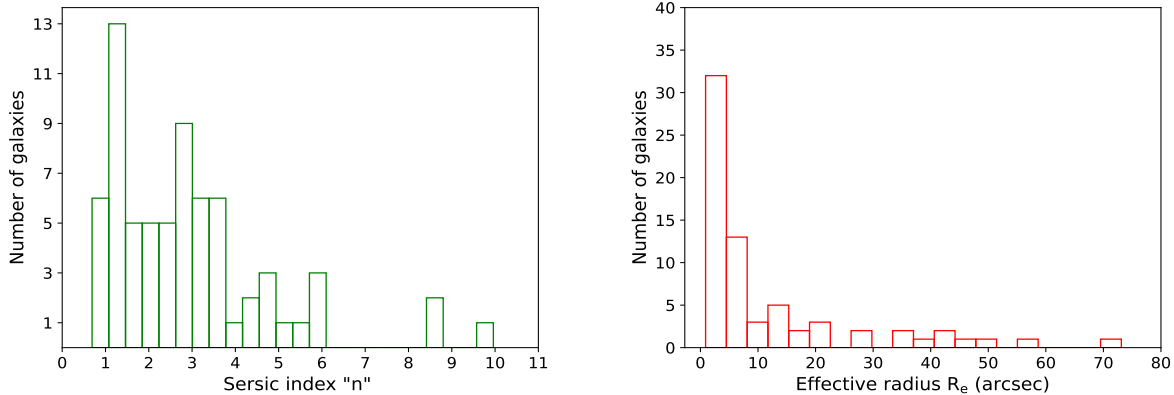


Figure 1. Distribution of the Sersic index (n) and effective radius R_e (arcsec) of the sample of elliptical and disk galaxies, obtained from single Sersic modeling by GALFIT. **Left:** Distribution of Sersic index (n). The no. of bins used to show the distribution is 24. We note that several visually identified spiral galaxies spuriously give $n > 2.5$, here. **Right:** Distribution of effective radius R_e . The no. of bins chosen here is 20.

disk etc). Thus, we discard 47 from the initial sample of 132. We then visually identify the totally edge-on disk galaxies (a total of 13), and do not use them in this work as it could be hard to identify double-disk in them robustly. This gives us a sample of elliptical galaxies and disk galaxies upto moderate inclination (a total of 72). Now, in order to determine the disk galaxies from the above sample, we perform 2D GALFIT modeling (Peng et al. 2002, 2010) of each galaxy. We fit a single Sersic model, using GALFIT, on the synthetic g-band images of the galaxies. The output of the GALFIT modeling consists of the best-fit Sersic model parameters (Sersic index "n", effective radius R_e , axis ratio, position angle, center coordinates). We consider the galaxies with Sersic index $n < 2.5$ to be disk galaxies, and the galaxies with $n > 2.5$ to be ellipticals (Shen et al. 2003; Lange et al. 2015; Sachdeva et al. 2020). We also checked that in some cases the single sersic model spuriously gives $n > 2.5$ for galaxies that contain prominent spiral structure or ring, leading them to be misclassified as ellipticals in the above process. Therefore, we finalise the number of disk galaxies to be 57, and elliptical galaxies to be 15, based on GALFIT modeling as well as visual inspection of the galaxy images wherever necessary. We use this sample of disk galaxies to find out the ones that have a double-exponential disk structure.

We show the distribution of the Sersic index "n" and effective radius " R_e ", corresponding to the best-fit single Sersic model of the ellipticals and disk galaxies in Fig.1, except three cases where the GALFIT result either did not converge or produced extremely high value of R_e .

2.3. GALFIT modeling of the disk galaxies

To find out the galaxies that contain two exponential disks, among the sample of 57, we perform GALFIT

modeling of each of them using a sersic plus single exponential profile, in the first step. The sersic function typically models the central bulge/bar component, and the exponential function models the disk component. For simplicity, we do not aim to model the spiral structure or star-forming rings in the galaxies. Now, GALFIT output gives us the best-fit model images as well as the corresponding residual images that are constructed by subtracting the model from the input data. The galaxies that have two exponential disks would leave an overall positive residue in the residual maps, especially toward the outer disk region of the galaxy. Now, instead of visually analysing each of the 57 residual images, we make histogram of the residual distributions of each case. The galaxies having any additional component would give rise to a positively biased histogram. We note that, this could be a useful technique while exploring a very large number of galaxies from both simulated as well as observed dataset where visual analysis of the large number of residual images could be a very tedious process. We chose 46 galaxies showing a positively biased, extended distribution of residual in their histograms and fit them with a second exponential disk using GALFIT. We then carefully inspect the resulting residual images of the above galaxies one-by-one to understand if the positive residue present in the previous sersic plus single exponential disk model, specifically in the outer disk regime of the galaxies, is now reduced and randomised due to the addition of the second disk component. We do not expect any significant change in the central part of the residual map as the second disk component present in the galaxy, if any, would make very small change in the central regime due to its faint surface brightness.

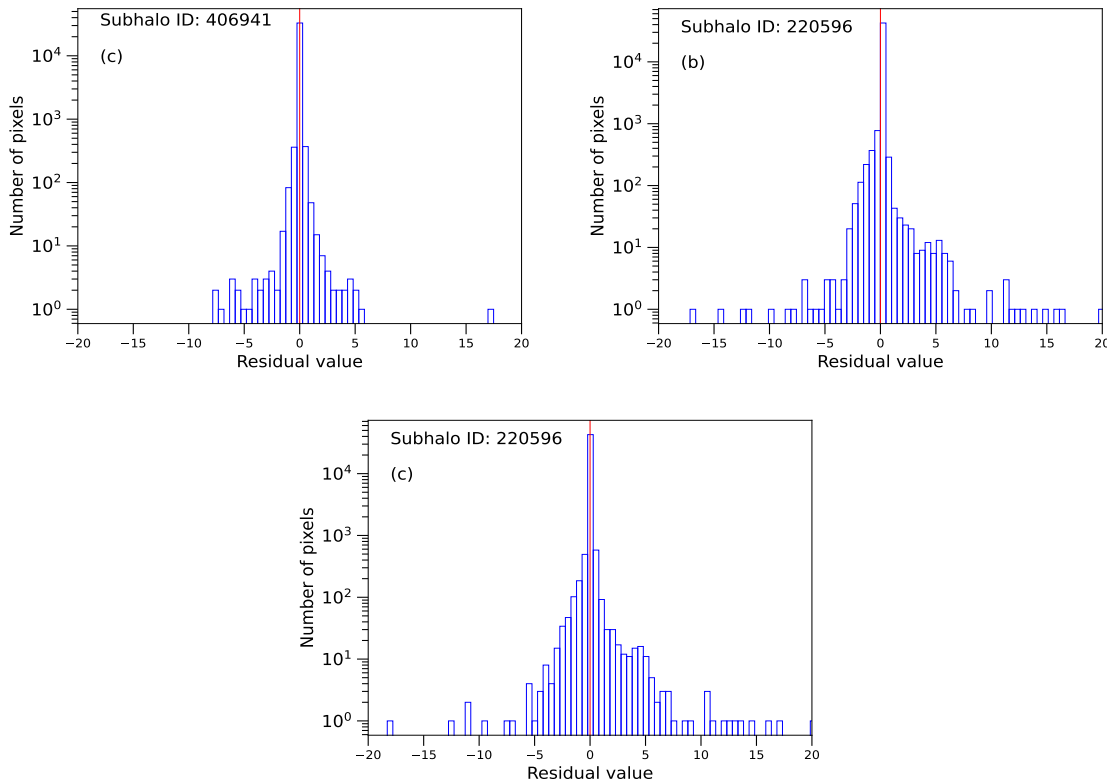


Figure 2. Histogram of distribution of GALFIT residual for two galaxies in the synthetic SDSS-g band. For the purpose of comparison, the range of x-axis is taken to be the same in each case. The red vertical line, passing through the zero value of residual, separates the positive and negative residual. **Panel (a):** showing a symmetric histogram for subhalo ID:406941 fitted with Sersic plus exponential. **Panel (b):** The same for subhalo ID: 220596 which reveals positive skewness - a case for double disk model. **Panel (c):** Same as in panel (b) but with a Sersic plus two exponential disks. The histogram here clearly appears to be more symmetric upon addition of an extended low surface brightness disk.

Based on the above process of visual analysis, and the decreased value of the reduced chi-square compared to that in the corresponding sersic plus single disk fit model, we conclude seven galaxies to be best represented by a sersic plus two exponential disks. We consider this sample as our sample of double-disk galaxies in this paper.

We show the histogram of distribution of the GALFIT residual of one single-disk and one double-disk galaxy in Figure 2. For the sake of convenience, we also present a flowchart (Figure 3) showing the main steps followed in this paper to detect the double disk galaxies from our initial mass-selected sample. We study various properties of the double-disk galaxies in the following section.

3. RESULTS

3.1. Structural properties of the double-disk galaxies

We present the GALFIT modeling results obtained for the double-disk galaxies in Figure 4. The input images are shown in the leftmost column, and the residual images obtained from the corresponding GALFIT mod-

eling are shown in the rightmost column. We note, that the spiral structure, that have not been modeled with any analytical function using GALFIT, are present very clearly in the residual images. We also calculate the 1D surface brightness profile (red data points in Fig.4) of the double-disk galaxies by running IRAF ELLIPSE task (Jedrzejewski 1987) on their g-band images, and show the profiles in the middle column. We then overplot the best-fit central sersic, inner & outer exponential disk profiles, using the results obtained from GALFIT (calculations are described below), on those 1-D surface brightness profiles. We note that, the total, i.e. analytical sum of those component profiles (black curve) reproduce the 1-D surface brightness profile well. Thus both 2D light modeling and 1-D surface brightness profile of the galaxies bring out the presence of double-disk in them.

GALFIT model result gives us the integrated apparent magnitude (m_{Sersic}), effective radius (R_e) of the best-fit central Sersic model. We use these to calculate the effective surface brightness (μ_e) and the central surface

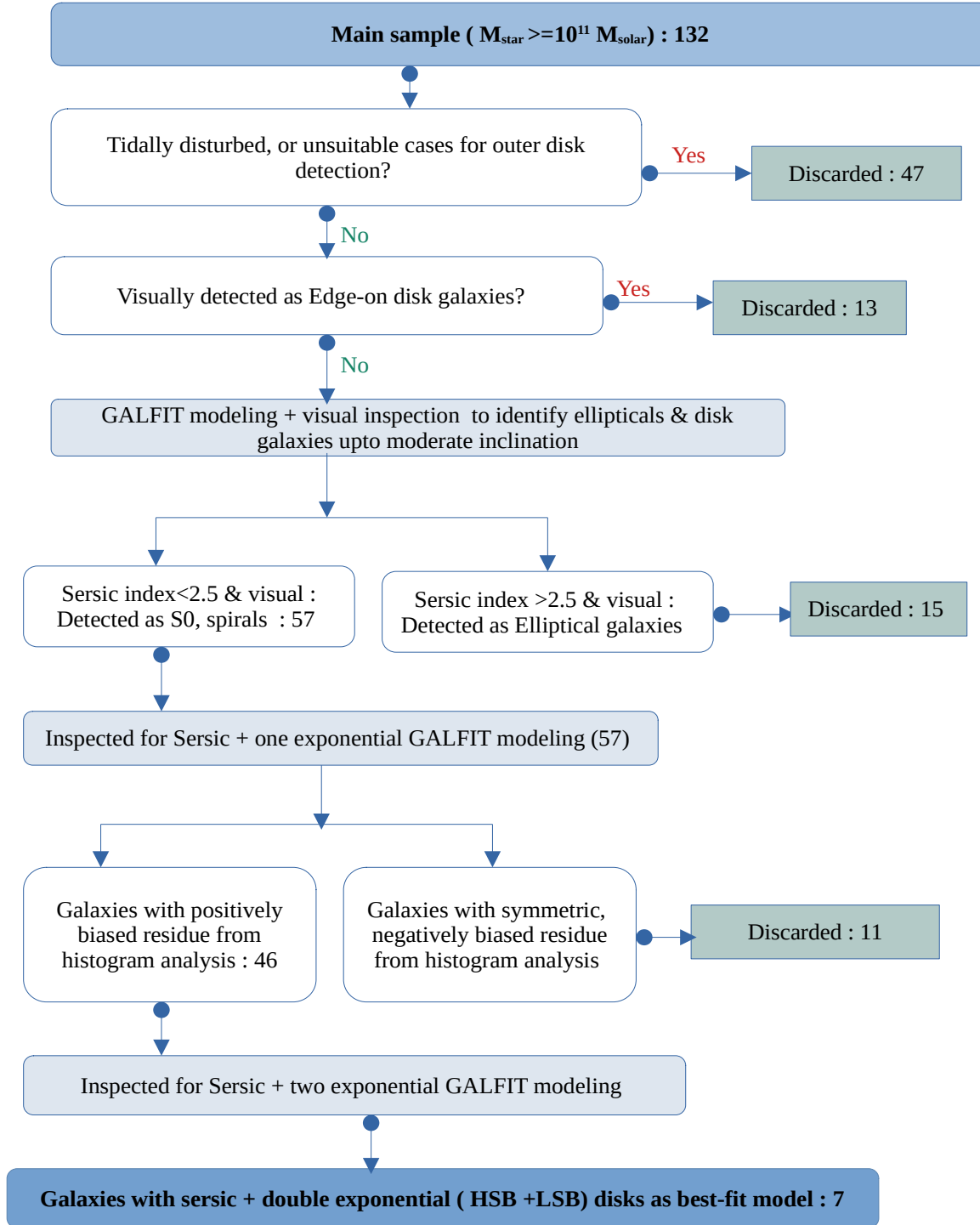


Figure 3. Flowchart to represent the steps followed to detect the double exponential disk galaxies from the sample of massive galaxies from TNG50 data.

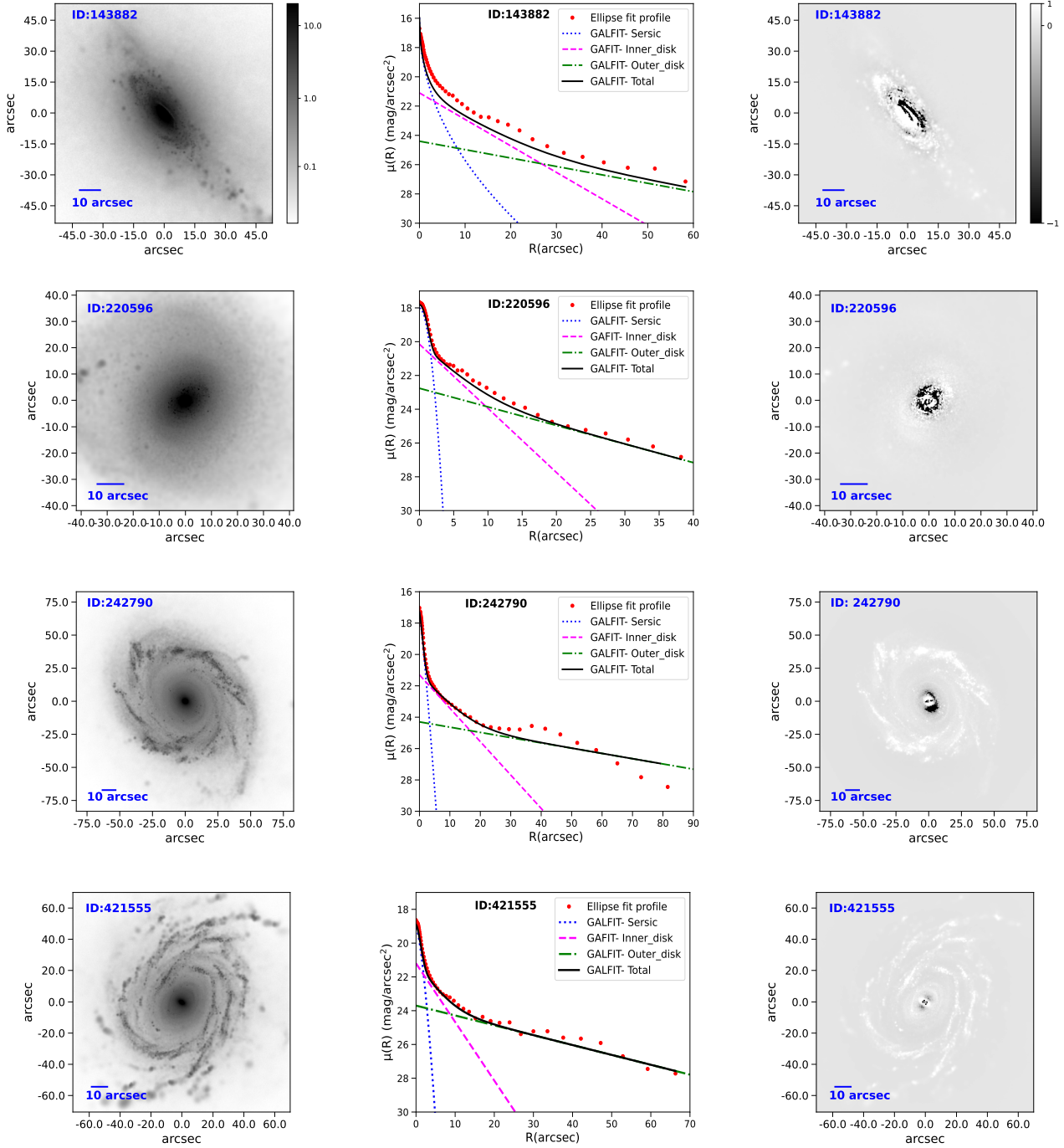


Figure 4. Massive galaxies (subhaloes) with double-exponential i.e., HSB plus LSB disk structures. The subhalo IDs are mentioned in each case. All the images are displayed in negative gray scale, in image unit. **Left column:** Synthetic SDSS g-band idealised images, shown using the same color bar (in log stretch). **Middle column:** Plot of the 1D surface brightness profiles (red data points) obtained from elliptical isophote fitting of the input images. The best-fit central sersic (blue dotted curve), inner (magenta dashed curve) and outer exponential (green dash-dotted curve) disk profiles, calculated analytically from the corresponding best-fit 2D GALFIT model, are over-plotted on the above 1-D surface brightness profiles. The total, i.e., the analytical sum of the GALFIT model profiles (black solid curve), agrees well with the 1-D profile of each galaxy. **Right column:** Residual images obtained from GALFIT modeling. The images are displayed following the same color bar (in log stretch).

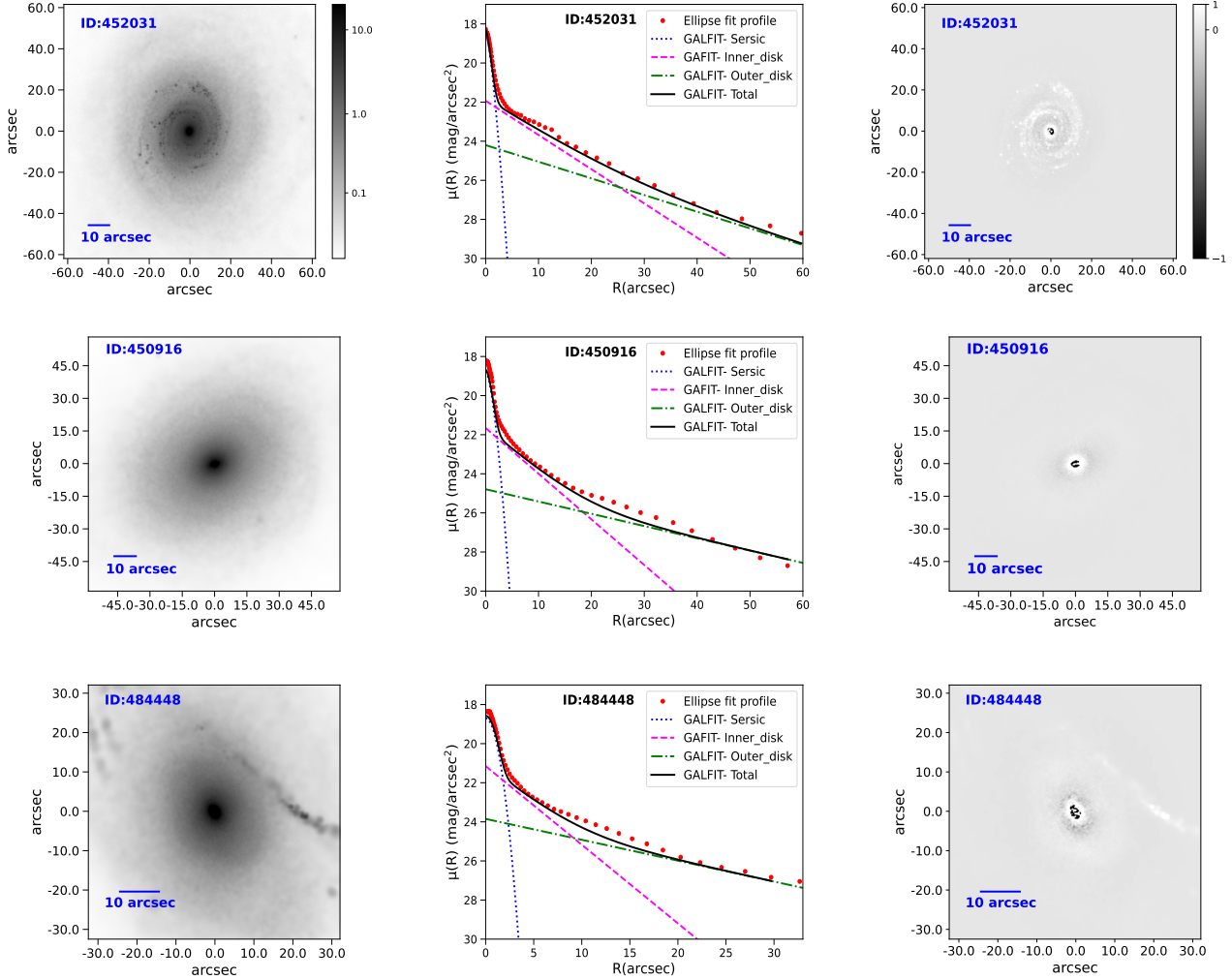


Figure 4. Continued from the above figure

brightness ($\mu_{0,seraic}$) of the Sersic component, using the following two equations.

$$\mu_e = m_{seraic} + 5\log_{10}R_e + 2.5\log_{10}\left(2\pi n \frac{e^{b_n}}{(b_n)^{2n}} \Gamma(2n)\right)$$

$$\mu_{0,seraic} = \mu_e - \frac{2.5b_n}{\ln(10)}$$

where $b_n = 1.9992n - 0.3271$ for $0.5 < n < 10$ (Capaccioli 1989; Graham & Driver 2005).

Similarly, we use integrated apparent magnitudes of the inner and the outer exponential disk components (m_{disk}), and their corresponding scale lengths (R_D), obtained from GALFIT, to calculate their central surface brightness values as follows

$$\mu_{0,disk} = m_{disk} + 2.5\log_{10}(2\pi R_D^2)$$

Finally we use the following analytical expressions to calculate the radial surface brightness profiles corre-

sponding to Sersic and exponential functions (Graham & Driver 2005; Graham & Worley 2008).

$$\mu_{seraic}(R) = \mu_e + \frac{2.5b_n}{\ln(10)} [(R/R_e)^{1/n} - 1]$$

$$\mu_{disk}(R) = \mu_{0,disk} + 1.086 \left(\frac{R}{R_D}\right).$$

We over-plot the above profiles on the 1-D surface brightness profile obtained from ellipse fitting in Figure 4.

Next, we correct $\mu_{0,disk}$ values for inclination using the axis ratio of the disk (obtained as a best-fit parameter from GALFIT modeling), and for cosmological surface brightness dimming effect (since by construction the images include this effect (Rodriguez-Gomez et al. 2019)), using the following equation (Zhong et al. 2008; Pahwa & Saha 2018)

$$\mu_{0,c} = \mu_0 + 2.5\log_{10}(b/a) - 10\log_{10}(1+z)$$

Table 2. Structural parameters of the double-exponential disk galaxies calculated from the GALFIT model results. The central surface brightness ($\mu_{0,\text{seraic}}$), effective radius (R_e) and sersic index ('n') of best-fit Sersic profile, and the central surface brightness, radial scale lengths of the inner & outer exponential disk profiles ($\mu_{0,\text{ID}}$, $\mu_{0,\text{OD}}$, $R_{\text{D,ID}}$, $R_{\text{D,OD}}$) are given.

| Subhalo ID | Central component (Bulge/bar) | | | Inner disk (ID) | | Outer disk (OD) | |
|-----------------|--|-------------------|------|--|-------------------------------|--|-------------------------------|
| | Sersic | | | Exponential | | Exponential | |
| | $\mu_{0,\text{seraic}}$ (mag.arcsec ⁻²) | R_e (arcsec) | n | $\mu_{0,\text{ID}}$ (mag.arcsec ⁻²) | $R_{\text{D,ID}}$ (arcsec) | $\mu_{0,\text{OD}}$ (mag.arcsec ⁻²) | $R_{\text{D,OD}}$ (arcsec) |
| SDSS g-band | | | | | | | |
| 143882 | 15.97 | 1.7 | 2.1 | 20.2 | 6.0 | 23.5 | 18.9 |
| 220596 | 18.06 | 0.85 | 0.5 | 19.6 | 2.86 | 22.4 | 9.9 |
| 242790 | 17.32 | 0.89 | 0.86 | 20.8 | 5.1 | 23.94 | 32.4 |
| 421555 | 19.07 | 1.04 | 0.67 | 20.93 | 3.13 | 23.4 | 18.6 |
| 450916 | 18.8 | 1.0 | 0.62 | 21.1 | 4.6 | 24.4 | 17.3 |
| 452031 | 18.3 | 0.91 | 0.72 | 21.5 | 6.2 | 23.8 | 12.75 |
| 484448 | 18.7 | 0.87 | 0.50 | 20.7 | 2.7 | 23.4 | 10.2 |
| SDSS r-band | | | | | | | |
| 143882 | 15.1 | 1.72 | 2.1 | 19.4 | 6.0 | 23.3 | 18.9 |
| 220596 | 17.1 | 0.86 | 0.5 | 18.8 | 2.86 | 21.6 | 9.9 |
| 242790 | 16.4 | 0.89 | 0.86 | 19.94 | 5.11 | 23.3 | 32.4 |
| 421555 | 18.08 | 1.01 | 0.66 | 20.09 | 3.14 | 22.6 | 15.8 |
| 450916 | 17.9 | 1.0 | 0.62 | 20.3 | 4.6 | 23.7 | 17.9 |
| 452031 | 17.4 | 0.91 | 0.72 | 20.73 | 5.4 | 22.35 | 10.9 |
| 484448 | 17.8 | 0.87 | 0.50 | 19.93 | 2.6 | 22.2 | 9.25 |
| Optical B- band | | | | | | | |
| 143882 | ... | ... | ... | 20.8 | ... | 23.8 | ... |
| 220596 | ... | ... | ... | 20.2 | ... | 22.96 | ... |
| 242790 | ... | ... | ... | 21.4 | ... | 24.4 | ... |
| 421555 | ... | ... | ... | 21.5 | ... | 23.8 | ... |
| 450916 | ... | ... | ... | 21.7 | ... | 24.8 | ... |
| 452031 | ... | ... | ... | 22.0 | ... | 24.65 | ... |
| 484448 | ... | ... | ... | 21.2 | ... | 24.1 | ... |

where $z = 0.0485$, as discussed in Section 2.2.1.

Finally, we determine the B-band central surface brightness values of the disk components using the equation below (Smith et al. 2002; Pahwa & Saha 2018).

$$\mu_0(B) = \mu_{0,c}(g) + 0.47(\mu_{0,c}(g) - \mu_{0,c}(r)) + 0.17$$

We present the structural parameters calculated above, corresponding to g, r, B bands, in Table 2.

A galaxy disk is identified as a low surface brightness disk if its B-band central surface brightness is fainter than 22.5 mag.arcsec⁻² (McGaugh 1996; Rosenbaum et al. 2009) which is an widely used criteria in literature. This shows that the inner disk of our sample of double-disk galaxies are HSB components while the outer disks indeed satisfy the LSB disk determination criteria.

Interestingly, the structural parameters of the HSB & LSB disk components calculated for our double-disk

galaxies fall within the range of that of the observed double-disk galaxies as given in Table 1. This shows that the simulated massive, double-exponential galaxies are morphologically good representative of the observed double-disk galaxies. In each case, the extended LSB disk has a radial scale length more than 10 kpc (except ID: 220596, 484448 that have slightly smaller scale length). Therefore, these double-disk galaxies could be considered as a giant low surface brightness galaxy, according to the definition of a gLSB (Das 2013; Saburova et al. 2023; Zhu et al. 2023). Although, note that the overall radial extent of the subhalo IDs: 220596, 484448 are significantly smaller than that of a typical gLSB.

Interestingly, although the volume fraction of gLSB galaxies in the local universe ($z < 0.1$) has been predicted through both observation and simulation (Saburova et al. 2023; Zhu et al. 2023) these papers do not explore the corresponding number for the galaxies with

double-disk morphology. Our result shows that, from simulation we are able to detect 7 massive disk galaxies with double-exponential disk morphology out of a total 57 massive disk galaxies, i.e, 12% of the parent sample, present in a simulation volume of $\sim 50^3$ Mpc³.

3.2. Color profiles and star formation property

We obtain the radial profile of the (g-r) optical color for each galaxy (Figure 5) using the azimuthally averaged flux per pixel calculated within concentric circular annulus placed over the corresponding SDSS-(g-r) color maps. We note that the color profile usually decreases from a maximum at the center to a minimum, and then rises again and attain a flat part. Overall, the central part of each galaxy appears to be the reddest, with $(g-r) \geq 0.8$ in all cases studied here - indicating a redder bulge/bar component associated with a bluer disk. In literature, this has been shown for local spirals (Morselli et al. 2017; Barsanti et al. 2021). The striking feature of some of these double disk galaxies appears to be their color minima. We do not find any apparent correlation between the radii corresponding to the color minima and the radii from which LSB disks start to dominate the surface brightness profile.

In the following, we explore the star formation property of the double-disk galaxies. The specific star formation rate, i.e, the ratio of the rate of current star formation to the stellar mass, shows a bi-modality in the sSFR vs. M_{star} plane, also manifested in their color-magnitude relation for the observed local galaxies (Kauffmann et al. 2003; Baldry et al. 2006; Dekel & Birnboim 2006; Ilbert et al. 2015). On this plane, the main sequence star-forming galaxies lie above $\log(\text{sSFR}) \geq -10.8 \text{ yr}^{-1}$, the quenched galaxies with very little or no star formation lie below $\log(\text{sSFR}) < -11.8 \text{ yr}^{-1}$, and the galaxies lying between these two regions are termed as the green-valley galaxies (Schawinski et al. 2014; Barway & Saha 2020). We show the simulated double-disk galaxies, the sample of 132 massive galaxies, and all the simulated galaxies with $M_{\text{star}} > 10^9 M_{\odot}$ from TNG50-1 on the sSFR vs. M_{star} plane in the backdrop of observed local galaxies in Figure 6. The data for the observed galaxies from SDSS observation, are taken from the catalogue by Salim et al. (2016). The stellar mass, and SFR of the observed galaxies calculated as a time-averaged quantity over last 100 Myr, are obtained from their SED Modeling in the catalogue. The density contours plotted on this background sample clearly shows the bi-modality in sSFR. The SFR data of all the simulated galaxies are taken from the supplementary data catalogue available on TNG website (Donnari et al. 2019; Pillepich et al. 2019). We consider the subhalo SFR calculated using

all the gravitationally bound stars of the subhalo, and time-averaged across the last 100 Myr, from the above catalogue. Using this SFR value and the total stellar mass of each subhalo (as has been consistently used in this paper) we then determine the sSFR of each simulated galaxy. Among the sample of the double-disk galaxies, we find one (ID:421555) to be at just the edge of the star-forming region, one (Subhalo ID: 484448) to be in the quenched region, and the rest of the four galaxies (Subhalo IDs: 143882, 220596, 242790, 452031) to lie in the green-valley region of the observed sample. The subhalo ID: 450916 does not have a resolved SFR value due to the finite numerical resolution of the simulation. It has been artificially assigned a zero value for SFR in the catalogue, and therefore it does not appear in the plot (Donnari et al. 2019). We also note that, the sample of TNG50-1 galaxies with $M_{\star} > 10^9 M_{\odot}$ do not show a strong bi-modality (for a detailed discussion see Donnari et al. (2019)).

3.3. Tully-Fisher relation

The Tully-Fisher relation (Tully & Fisher 1977; Bell & de Jong 2001; Courteau et al. 2003; den Heijer et al. 2015) is the correlation between the mass of a disk galaxy and its rotation velocity. This has been shown to be one of the most fundamental galaxy scaling relations for disk galaxies, in observations so far. This can be studied in terms of stellar mass, i.e, galaxy luminosity vs. rotation velocity (Tully & Fisher 1977) as well as the total baryonic mass (stars+gas) vs. rotation velocity. The baryonic Tully-Fisher relation provides a much stronger correlation than the stellar mass Tully-Fisher relation, with much reduced scatter (McGaugh et al. 2000; Gurovich et al. 2004; McGaugh 2005; Trachtenbach et al. 2009). The linear slope of the BTFR is usually observed to lie in the range of 3-4. In this work, we explore the BTFR of the massive disk (57) galaxies in our sample, including the double-disk cases, in Figure 7. As the observational sample, we consider the BTFR for late-type disk galaxies studied in Lelli et al. (2019), based on SPARC dataset (Lelli et al. 2016), using maximum rotation velocity (V_{max}), which resulted into a slope of 3.52 ± 0.07 in their paper. We show the 1.5- σ region (grey shaded region) of the observed BTFR, calculated using the corresponding values reported in their paper, in the figure. We use the gravitationally bound total baryonic mass (stars+gas), and V_{max} , i.e, the maximum of the spherically averaged rotation curve of the simulated galaxies, available in the TNG SUBFIND data catalogue, and show these on the same figure. Interestingly, all the double-disk galaxies are found to lie within the 1.5- σ region of the observed BTFR, except two (Sub-

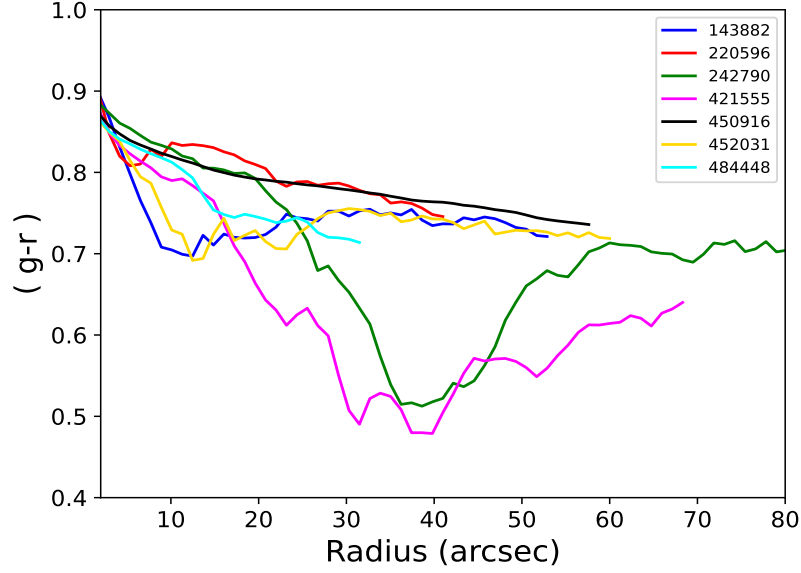


Figure 5. Plot of $g-r$ color profile vs. radius of the double-disk galaxies obtained from their corresponding synthetic SDSS- g,r band images.

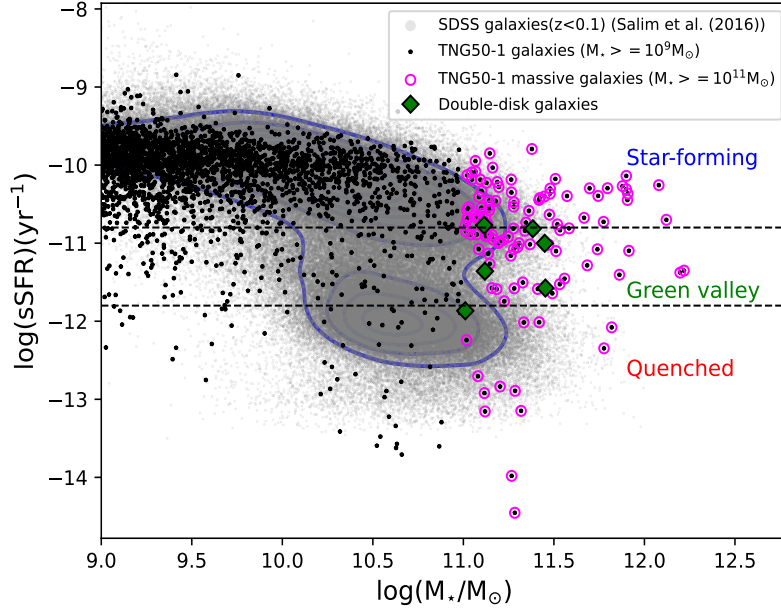


Figure 6. Specific star formation rate (sSFR) vs. M_* : The background galaxies represented by grey dots are the observed local galaxies from SDSS observation. The sSFR vs M_* plane is divided into three regions: star-forming ($\log(\text{sSFR}) \geq -10.8$), green-valley ($-10.8 > \log(\text{sSFR}) > -11.8$) and quenched ($\log(\text{sSFR}) \leq -11.8$) (see Barway & Saha 2020). The black points represent all TNG50-1 galaxies with total $M_* > 10^9 M_\odot$ with resolved SFR. The 132 massive galaxies used in our work are marked by the magenta circles. The double-disk galaxies are marked by the green diamonds among them. The subhalo ID: 421555 lies at the edge of the star-forming region, ID: 484448 is in the quenched region. The rest of the double-disk galaxies (143882, 220596, 242790, 452031) are in the green-valley region except ID: 450916 which has an unresolved SFR value and is, therefore, assigned SFR=0 in the data catalogue.

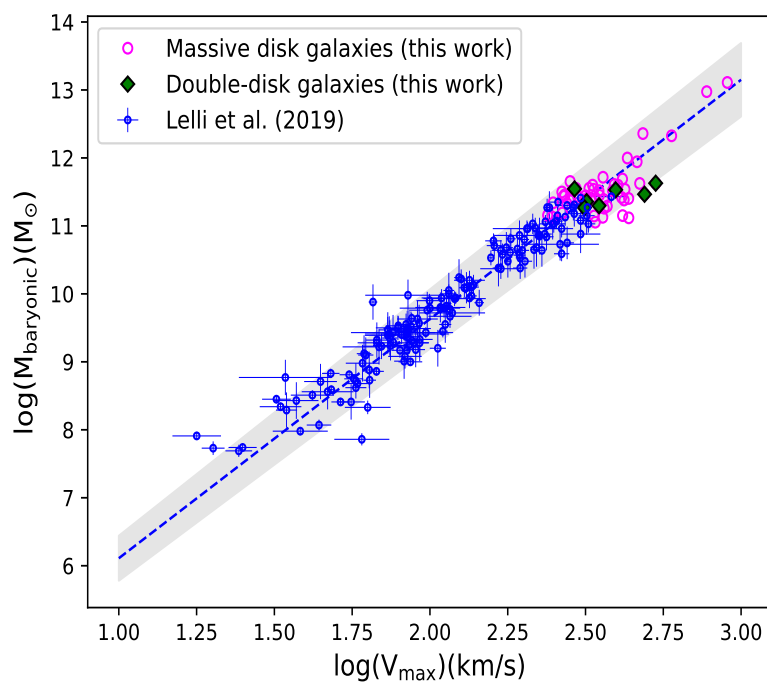


Figure 7. Baryonic Tully-Fisher relation: The magenta circles represent the sample of 57 massive simulated disk galaxies used in our work. We mark the double-disk galaxies among them with green diamonds. The blue circles represent observed disk galaxies, studied by Lelli et al. (2019). This sample follows the BTFR (blue dashed line) with a slope of 3.52 ± 0.07 & intercept of 2.59 ± 0.15 , as reported in their paper. The grey shaded region represents $1.5\text{-}\sigma$ region of the above observed BTFR.

halo IDs: 143882, 220596) which lie just at the edge of the region.

4. CONCLUSION

We have studied massive disk galaxies from the highest resolution run of IllustrisTNG50 simulation in order to find out galaxies with a double-exponential disk morphology where the second disk is a low surface brightness component surrounding the central high surface brightness inner disk component. We used the idealised, synthetic SDSS *g*, *r* band images of the galaxies, available in the TNG supplementary data catalogue, to do detailed 2D structural decomposition. We summarize the main results from our paper as follows.

- We detect 7 double-exponential disk galaxies, which is $\sim 12\%$ of the 57 disk galaxies from TNG50 chosen for GALFIT modeling.
- The central surface brightness values of the inner and outer exponential disks lie in the range of 20.2- 22.0 mag.arcsec⁻² & 23-24.8 mag.arcsec⁻², respectively, in optical B-band. The radial scale lengths of the disks lie in the range of 2.6-6.1 kpc & 9.7-31.7 kpc, respectively, corresponding to SDSS *g* band. These values are in agreement with those in observed double-disk galaxies.
- Using TNG supplementary data catalogue, we studied the time-averaged (over last 100 Myr) specific star formation rate of the double-disk galaxies. One of the double-disk galaxies lies in the edge of the star-forming region, one lies in the quenched region, and the rest of the sample lie in the green-valley region compared to the observed local ($z < 0.1$) SDSS galaxies. We found one double-disk galaxy in our sample to have an unresolved SFR value.

- We measure radial optical color profiles of the galaxies which usually show a global minimum along the galactocentric radius. There is no apparent correlation between the radii corresponding to the color minima and the radii from which the LSB disk starts to dominate the surface brightness profile.

- Interestingly, the double-disk galaxies along with the massive disk galaxies are found to lie within the 1.5σ region of the observed Baryonic Tully-Fisher relation.

Massive disk galaxies with such layered structure invoke many intriguing questions in the context of formation of massive disk galaxies, growth of the LSB envelope, and their existence at $z=0$. This could be explored only by constructing a statistically large sample. The detection of such galaxies in observation are small in number till date. Our results obtained from simulations could serve as a motivation to look for such galaxies in deep photometric observations such as from HSC-SSP (Hyper Suprime Cam - Subaru Strategic Program)(Aihara et al. 2022), as well as from the upcoming data from LSST (Large Synoptic Survey Telescope) (Ivezić et al. 2019).

ACKNOWLEDGEMENTS

This research done in this paper has used data from IllustrisTNG simulation publicly available on the IllustrisTNG website, and data from the publicly available SPARC (Spitzer Photometry & Accurate Rotation Curves) database (Lelli et al. 2016). Software: GALFIT, IRAF, Astropy, DS9.

REFERENCES

- Abraham, R. G., & van Dokkum, P. G. 2014, *PASP*, 126, 55, doi: [10.1086/674875](https://doi.org/10.1086/674875)
- Aihara, H., Armstrong, R., Bickerton, S., et al. 2018, *PASJ*, 70, S8, doi: [10.1093/pasj/psx081](https://doi.org/10.1093/pasj/psx081)
- Aihara, H., AlSayyad, Y., Ando, M., et al. 2022, *PASJ*, 74, 247, doi: [10.1093/pasj/psab122](https://doi.org/10.1093/pasj/psab122)
- Baldry, I. K., Balogh, M. L., Bower, R. G., et al. 2006, *MNRAS*, 373, 469, doi: [10.1111/j.1365-2966.2006.11081.x](https://doi.org/10.1111/j.1365-2966.2006.11081.x)
- Barsanti, S., Owers, M. S., McDermid, R. M., et al. 2021, *ApJ*, 911, 21, doi: [10.3847/1538-4357/abe5ac](https://doi.org/10.3847/1538-4357/abe5ac)
- Barth, A. J. 2007, *AJ*, 133, 1085, doi: [10.1086/511180](https://doi.org/10.1086/511180)
- Barway, S., & Saha, K. 2020, *MNRAS*, 495, 4548, doi: [10.1093/mnras/staa1387](https://doi.org/10.1093/mnras/staa1387)
- Bell, E. F., & de Jong, R. S. 2001, *ApJ*, 550, 212, doi: [10.1086/319728](https://doi.org/10.1086/319728)
- Bothun, G. D., Impey, C. D., Malin, D. F., & Mould, J. R. 1987, *AJ*, 94, 23, doi: [10.1086/114443](https://doi.org/10.1086/114443)
- Capaccioli, M. 1989, in *World of Galaxies (Le Monde des Galaxies)*, ed. J. Corwin, Harold G. & L. Bottinelli, 208–227
- Courteau, S., Andersen, D. R., Bershad, M. A., MacArthur, L. A., & Rix, H.-W. 2003, *ApJ*, 594, 208, doi: [10.1086/376754](https://doi.org/10.1086/376754)

- Das, M. 2013, *Journal of Astrophysics and Astronomy*, 34, 19, doi: [10.1007/s12036-013-9166-8](https://doi.org/10.1007/s12036-013-9166-8)
- Dekel, A., & Birnboim, Y. 2006, *MNRAS*, 368, 2, doi: [10.1111/j.1365-2966.2006.10145.x](https://doi.org/10.1111/j.1365-2966.2006.10145.x)
- den Heijer, M., Oosterloo, T. A., Serra, P., et al. 2015, *A&A*, 581, A98, doi: [10.1051/0004-6361/201526879](https://doi.org/10.1051/0004-6361/201526879)
- Di Cintio, A., Brook, C. B., Macciò, A. V., Dutton, A. A., & Cardona-Barrero, S. 2019, *MNRAS*, 486, 2535, doi: [10.1093/mnras/stz985](https://doi.org/10.1093/mnras/stz985)
- Donnari, M., Pillepich, A., Nelson, D., et al. 2019, *MNRAS*, 485, 4817, doi: [10.1093/mnras/stz712](https://doi.org/10.1093/mnras/stz712)
- Genel, S., Vogelsberger, M., Springel, V., et al. 2014, *MNRAS*, 445, 175, doi: [10.1093/mnras/stu1654](https://doi.org/10.1093/mnras/stu1654)
- Graham, A. W., & Driver, S. P. 2005, *PASA*, 22, 118, doi: [10.1071/AS05001](https://doi.org/10.1071/AS05001)
- Graham, A. W., & Worley, C. C. 2008, *MNRAS*, 388, 1708, doi: [10.1111/j.1365-2966.2008.13506.x](https://doi.org/10.1111/j.1365-2966.2008.13506.x)
- Gurovich, S., McGaugh, S. S., Freeman, K. C., et al. 2004, *PASA*, 21, 412, doi: [10.1071/AS04038](https://doi.org/10.1071/AS04038)
- Hagen, L. M. Z., Seibert, M., Hagen, A., et al. 2016, *ApJ*, 826, 210, doi: [10.3847/0004-637X/826/2/210](https://doi.org/10.3847/0004-637X/826/2/210)
- Ilbert, O., Arnouts, S., Le Floch, E., et al. 2015, *A&A*, 579, A2, doi: [10.1051/0004-6361/201425176](https://doi.org/10.1051/0004-6361/201425176)
- Impey, C., & Bothun, G. 1989, *ApJ*, 341, 89, doi: [10.1086/167474](https://doi.org/10.1086/167474)
- Ivezić, Ž., Kahn, S. M., Tyson, J. A., et al. 2019, *ApJ*, 873, 111, doi: [10.3847/1538-4357/ab042c](https://doi.org/10.3847/1538-4357/ab042c)
- Jackson, R. A., Kaviraj, S., Martin, G., et al. 2022, *MNRAS*, 511, 607, doi: [10.1093/mnras/stac058](https://doi.org/10.1093/mnras/stac058)
- Jackson, R. A., Martin, G., Kaviraj, S., et al. 2020, *MNRAS*, 494, 5568, doi: [10.1093/mnras/staa970](https://doi.org/10.1093/mnras/staa970)
- Jedrzejewski, R. I. 1987, *MNRAS*, 226, 747, doi: [10.1093/mnras/226.4.747](https://doi.org/10.1093/mnras/226.4.747)
- Kauffmann, G., Heckman, T. M., White, S. D. M., et al. 2003, *MNRAS*, 341, 33, doi: [10.1046/j.1365-8711.2003.06291.x](https://doi.org/10.1046/j.1365-8711.2003.06291.x)
- Kulier, A., Galaz, G., Padilla, N. D., & Trayford, J. W. 2020, *MNRAS*, 496, 3996, doi: [10.1093/mnras/staa1798](https://doi.org/10.1093/mnras/staa1798)
- LaChance, P., Croft, R., Ni, Y., et al. 2024, *arXiv e-prints*, arXiv:2401.16608, doi: [10.48550/arXiv.2401.16608](https://doi.org/10.48550/arXiv.2401.16608)
- Lange, R., Driver, S. P., Robotham, A. S. G., et al. 2015, *MNRAS*, 447, 2603, doi: [10.1093/mnras/stu2467](https://doi.org/10.1093/mnras/stu2467)
- Lelli, F., McGaugh, S. S., & Schombert, J. M. 2016, *AJ*, 152, 157, doi: [10.3847/0004-6256/152/6/157](https://doi.org/10.3847/0004-6256/152/6/157)
- Lelli, F., McGaugh, S. S., Schombert, J. M., Desmond, H., & Katz, H. 2019, *MNRAS*, 484, 3267, doi: [10.1093/mnras/stz205](https://doi.org/10.1093/mnras/stz205)
- Marinacci, F., Vogelsberger, M., Pakmor, R., et al. 2018, *MNRAS*, 480, 5113, doi: [10.1093/mnras/sty2206](https://doi.org/10.1093/mnras/sty2206)
- McGaugh, S. 1996, in *IAU Symposium*, Vol. 171, New Light on Galaxy Evolution, ed. R. Bender & R. L. Davies, 97, doi: [10.48550/arXiv.astro-ph/9507058](https://doi.org/10.48550/arXiv.astro-ph/9507058)
- McGaugh, S. S. 2005, *ApJ*, 632, 859, doi: [10.1086/432968](https://doi.org/10.1086/432968)
- McGaugh, S. S., Schombert, J. M., Bothun, G. D., & de Blok, W. J. G. 2000, *ApJL*, 533, L99, doi: [10.1086/312628](https://doi.org/10.1086/312628)
- Moore, L., & Parker, Q. A. 2006, *PASA*, 23, 165, doi: [10.1071/AS06022](https://doi.org/10.1071/AS06022)
- Morselli, L., Popesso, P., Erfanianfar, G., & Concas, A. 2017, *A&A*, 597, A97, doi: [10.1051/0004-6361/201629409](https://doi.org/10.1051/0004-6361/201629409)
- Naiman, J. P., Pillepich, A., Springel, V., et al. 2018, *MNRAS*, 477, 1206, doi: [10.1093/mnras/sty618](https://doi.org/10.1093/mnras/sty618)
- Nelson, D., Pillepich, A., Springel, V., et al. 2018, *MNRAS*, 475, 624, doi: [10.1093/mnras/stx3040](https://doi.org/10.1093/mnras/stx3040)
- . 2019, *MNRAS*, 490, 3234, doi: [10.1093/mnras/stz2306](https://doi.org/10.1093/mnras/stz2306)
- Pahwa, I., & Saha, K. 2018, *MNRAS*, 478, 4657, doi: [10.1093/mnras/sty1139](https://doi.org/10.1093/mnras/sty1139)
- Pandey, D., Saha, K., Pradhan, A. C., & Kaviraj, S. 2022, *ApJ*, 941, 128, doi: [10.3847/1538-4357/aca1c5](https://doi.org/10.3847/1538-4357/aca1c5)
- Peng, C. Y., Ho, L. C., Impey, C. D., & Rix, H.-W. 2002, *AJ*, 124, 266, doi: [10.1086/340952](https://doi.org/10.1086/340952)
- . 2010, *AJ*, 139, 2097, doi: [10.1088/0004-6256/139/6/2097](https://doi.org/10.1088/0004-6256/139/6/2097)
- Pérez-Montaño, L. E., Rodríguez-Gomez, V., Cervantes Sodi, B., et al. 2022, *MNRAS*, 514, 5840, doi: [10.1093/mnras/stac1716](https://doi.org/10.1093/mnras/stac1716)
- Pillepich, A., Springel, V., Nelson, D., et al. 2018a, *MNRAS*, 473, 4077, doi: [10.1093/mnras/stx2656](https://doi.org/10.1093/mnras/stx2656)
- Pillepich, A., Nelson, D., Hernquist, L., et al. 2018b, *MNRAS*, 475, 648, doi: [10.1093/mnras/stx3112](https://doi.org/10.1093/mnras/stx3112)
- Pillepich, A., Nelson, D., Springel, V., et al. 2019, *MNRAS*, 490, 3196, doi: [10.1093/mnras/stz2338](https://doi.org/10.1093/mnras/stz2338)
- Planck Collaboration, Ade, P. A. R., Aghanim, N., et al. 2016, *A&A*, 594, A13, doi: [10.1051/0004-6361/201525830](https://doi.org/10.1051/0004-6361/201525830)
- Rodríguez-Gomez, V., Snyder, G. F., Lotz, J. M., et al. 2019, *MNRAS*, 483, 4140, doi: [10.1093/mnras/sty3345](https://doi.org/10.1093/mnras/sty3345)
- Rosenbaum, S. D., Krusch, E., Bomans, D. J., & Dettmar, R. J. 2009, *A&A*, 504, 807, doi: [10.1051/0004-6361/20077462](https://doi.org/10.1051/0004-6361/20077462)
- Saburova, A. S., Chilingarian, I. V., Kasparova, A. V., et al. 2019, *MNRAS*, 489, 4669, doi: [10.1093/mnras/stz2434](https://doi.org/10.1093/mnras/stz2434)
- Saburova, A. S., Chilingarian, I. V., Kulier, A., et al. 2023, *MNRAS*, 520, L85, doi: [10.1093/mnras/520/l85](https://doi.org/10.1093/mnras/520/l85)
- Sachdeva, S., Ho, L. C., Li, Y. A., & Shankar, F. 2020, *ApJ*, 899, 89, doi: [10.3847/1538-4357/aba82d](https://doi.org/10.3847/1538-4357/aba82d)
- Saha, K., Dhiwar, S., Barway, S., Narayan, C., & Tandon, S. 2021, *Journal of Astrophysics and Astronomy*, 42, 59, doi: [10.1007/s12036-021-09715-5](https://doi.org/10.1007/s12036-021-09715-5)
- Salim, S., Lee, J. C., Janowiecki, S., et al. 2016, *ApJS*, 227, 2, doi: [10.3847/0067-0049/227/1/2](https://doi.org/10.3847/0067-0049/227/1/2)

- Schawinski, K., Urry, C. M., Simmons, B. D., et al. 2014, MNRAS, 440, 889, doi: [10.1093/mnras/stu327](https://doi.org/10.1093/mnras/stu327)
- Shen, S., Mo, H. J., White, S. D. M., et al. 2003, MNRAS, 343, 978, doi: [10.1046/j.1365-8711.2003.06740.x](https://doi.org/10.1046/j.1365-8711.2003.06740.x)
- Sijacki, D., Vogelsberger, M., Genel, S., et al. 2015, MNRAS, 452, 575, doi: [10.1093/mnras/stv1340](https://doi.org/10.1093/mnras/stv1340)
- Smith, J. A., Tucker, D. L., Kent, S., et al. 2002, AJ, 123, 2121, doi: [10.1086/339311](https://doi.org/10.1086/339311)
- Sprayberry, D., Impey, C. D., Bothun, G. D., & Irwin, M. J. 1995, AJ, 109, 558, doi: [10.1086/117300](https://doi.org/10.1086/117300)
- Springel, V. 2010, MNRAS, 401, 791, doi: [10.1111/j.1365-2966.2009.15715.x](https://doi.org/10.1111/j.1365-2966.2009.15715.x)
- Springel, V., White, S. D. M., Tormen, G., & Kauffmann, G. 2001, MNRAS, 328, 726, doi: [10.1046/j.1365-8711.2001.04912.x](https://doi.org/10.1046/j.1365-8711.2001.04912.x)
- Springel, V., Pakmor, R., Pillepich, A., et al. 2018, MNRAS, 475, 676, doi: [10.1093/mnras/stx3304](https://doi.org/10.1093/mnras/stx3304)
- Trachternach, C., de Blok, W. J. G., McGaugh, S. S., van der Hulst, J. M., & Dettmar, R. J. 2009, A&A, 505, 577, doi: [10.1051/0004-6361/200811136](https://doi.org/10.1051/0004-6361/200811136)
- Tully, R. B., & Fisher, J. R. 1977, A&A, 54, 661
- Vogelsberger, M., Genel, S., Springel, V., et al. 2014a, Nature, 509, 177, doi: [10.1038/nature13316](https://doi.org/10.1038/nature13316)
- . 2014b, MNRAS, 444, 1518, doi: [10.1093/mnras/stu1536](https://doi.org/10.1093/mnras/stu1536)
- Weinberger, R., Springel, V., Hernquist, L., et al. 2017, MNRAS, 465, 3291, doi: [10.1093/mnras/stw2944](https://doi.org/10.1093/mnras/stw2944)
- Zhang, J., Abraham, R., van Dokkum, P., Merritt, A., & Janssens, S. 2018, ApJ, 855, 78, doi: [10.3847/1538-4357/aaac81](https://doi.org/10.3847/1538-4357/aaac81)
- Zhong, G. H., Liang, Y. C., Liu, F. S., et al. 2008, MNRAS, 391, 986, doi: [10.1111/j.1365-2966.2008.13972.x](https://doi.org/10.1111/j.1365-2966.2008.13972.x)
- Zhu, Q., Pérez-Montaño, L. E., Rodríguez-Gomez, V., et al. 2023, MNRAS, 523, 3991, doi: [10.1093/mnras/stad1655](https://doi.org/10.1093/mnras/stad1655)
- Zhu, Q., Xu, D., Gaspari, M., et al. 2018, MNRAS, 480, L18, doi: [10.1093/mnrasl/sly111](https://doi.org/10.1093/mnrasl/sly111)